Colloids and Surfaces B: Biointerfaces 141 (2016) 291–300

Contents lists available at ScienceDirect

Colloids and Surfaces B: Biointerfaces

journal homepage: www.elsevier.com/locate/colsurfb

The importance of extracellular speciation and corrosion of copper nanoparticles on lung cell membrane integrity

Jonas Hedberg[a,*], Hanna L. Karlsson[b], Yolanda Hedberg[a], Eva Blomberg[a,c], Inger Odnevall Wallinder[a]

[a] KTH Royal Institute of Technology, School of Chemical Science and Engineering, Division of Surface and Corrosion Science, Drottning Kristinas v. 51, 100 44 Stockholm, Sweden
[b] Karolinska Institutet, Institute of Environmental Medicine, Unit of Biochemical Toxicology, Nobels väg 13, 17165 Stockholm, Sweden
[c] SP Technical Research Institute of Sweden, Chemistry, Materials and Surfaces, Stockholm, Sweden

ARTICLE INFO

Article history:
Received 16 September 2015
Received in revised form 26 January 2016
Accepted 27 January 2016
Available online 4 February 2016

Keywords:
Copper nanoparticles
Nanotoxicity
Lung cells
Speciation
Corrosion
Membrane damage
DMEM
Equilibrium modeling
UV–vis spectroscopy
Polarography

ABSTRACT

Copper nanoparticles (Cu NPs) are increasingly used in various biologically relevant applications and products, *e.g.*, due to their antimicrobial and catalytic properties. This inevitably demands for an improved understanding on their interactions and potential toxic effects on humans. The aim of this study was to investigate the corrosion of copper nanoparticles in various biological media and to elucidate the speciation of released copper in solution. Furthermore, reactive oxygen species (ROS) generation and lung cell (A549 type II) membrane damage induced by Cu NPs in the various media were studied. The used biological media of different complexity are of relevance for nanotoxicological studies: Dulbecco's modified eagle medium (DMEM), DMEM$^+$ (includes fetal bovine serum), phosphate buffered saline (PBS), and PBS + histidine. The results show that both copper release and corrosion are enhanced in DMEM$^+$, DMEM, and PBS + histidine compared with PBS alone. Speciation results show that essentially no free copper ions are present in the released fraction of Cu NPs in neither DMEM$^+$, DMEM nor histidine, while labile Cu complexes form in PBS. The Cu NPs were substantially more membrane reactive in PBS compared to the other media and the NPs caused larger effects compared to the same mass of Cu ions. Similarly, the Cu NPs caused much more ROS generation compared to the released fraction only. Taken together, the results suggest that membrane damage and ROS formation are stronger induced by Cu NPs and by free or labile Cu ions/complexes compared with Cu bound to biomolecules.

1. Introduction

The physico-chemical properties of nanoparticles (NPs), including copper nanoparticles (Cu NPs), can be tailored and controlled on the nanoscale by changing their characteristics, *e.g.*, size, surface capping, or shape [1,2]. As a consequence, the use of Cu NPs and their areas of applications rapidly increase. This increasing use demands for an improved understanding of potential adverse effects that may be an inevitable consequence of their interactions and transformations in biologically relevant settings. Such fundamental mechanistic knowledge is further essential from a human health and environmental risk perspective [3]. Adverse effects induced by the dispersion of Cu NPs have for example been shown on both human cells and on the environment [4,5].

Cu-containing NPs can induce toxicity *via* several different mechanisms [6–8], creating a situation more complicated compared with, *e.g.*, aqueous Cu species [9]. In addition to the particle effect, the chemical speciation of Cu species in solution (*e.g.*, released from Cu NPs) has been shown to significantly influence the observed toxicity. Free Cu ions and labile Cu complexes have been shown more potent compared with more strongly bound Cu complexes [10–13]. An additional mechanism that enhances the toxic effect of Cu NPs [6,14,15] is *via* the formation of reactive oxygen species (ROS) *via* electrochemical (oxidation) reactions [16,17], catalytic surface reactions [15,18] or *via* Fenton reactions of aqueous Cu species released from Cu NPs [19–21]. An important distinction between NPs of Cu oxides and Cu metal is hence the ability of Cu NPs to corrode forming ROS as intermediate products (cathodic reactions) [17,22]. Cell uptake of Cu-containing NPs can in addition induce damage through ROS production and via released Cu species within the cell (often denoted the Trojan horse-mechanism) [23,24].

* Corresponding author.
E-mail address: jhed@kth.se (J. Hedberg).

http://dx.doi.org/10.1016/j.colsurfb.2016.01.052

Some investigations have identified released Cu species as the main reason for observed toxicity of Cu NPs, [25,26] whereas other studies have concluded such species to be of minor importance [18,27,28]. These observations may not be in direct conflict with each other, as both fluid specifics and loading (mass Cu/volume) will largely influence the speciation and amount of released Cu, and hence, their individual importance. Despite the significance of the chemical speciation of released Cu on the observed toxic response, detailed understanding of this matter is mostly lacking in commonly used cell media, such as the Dulbecco's Modified Eagle Medium (DMEM).

This paper aims to fill this evident knowledge gap by: (i) providing chemical speciation information on Cu released from Cu NPs at extracellular conditions (in cell media—DMEM), (ii) deducing the correlation between chemical speciation of released Cu (possible labile Cu species) and membrane damage, ROS production, and corrosion of Cu NPs, and (iii) suggesting a model that elucidates Cu NPs-induced membrane damage in dependence of chemical speciation of released Cu in media of different Cu complexation capacity. A multi-analytical approach using polarography, UV–vis spectroscopy, and chemical equilibrium modeling (JESS, Joint Expert speciation system) has been employed to gain insight on the chemical speciation of Cu released from Cu NPs. Experimental studies have been performed in $DMEM^+$ (DMEM with added fetal bovine serum (FBS), penicillin, streptomycin, and pyruvate) to investigate the influence of protein-containing serum on the Cu speciation. Histidine solutions were selected as this amino acid has been reported to induce more Cu release from CuO NPs compared with other amino acids [21]. Phosphate buffered saline (PBS), a medium without any biomolecule constituents, was investigated for comparative reasons. In parallel, the membrane integrity (Trypan blue assay) of A549 (type II) lung cells was investigated following exposures to Cu NPs or Cu ions (from $Cu(NO_3)_2$), and the production of acellular ROS was monitored using the dichlorodihydrofluorescin diacetate (DCFH-DA) assay.

A previous investigation speculates that the reason for the higher cell membrane damage observed for Cu NPs compared with NPs of CuO is related to corrosion reactions taking place at the surface of the Cu NPs [16]. The corrosion behavior of the Cu NPs was therefore investigated using a carbon paste electrode (CPE) [29], monitoring the open circuit potential (OCP) to provide additional insights on the correlation between corrosion, induced toxicity, and the release of Cu species. It is, to the knowledge of the authors, the first time that CPE has been used in nanotoxicological investigations.

2. Materials and methods

2.1. Solutions and chemicals

DMEM (Dulbecco's modified eagle medium) was purchased from Life Technologies (Sweden, Lot# 1644395). For $DMEM^+$, 10 vol.% of fetal bovine serum (Gibco®, Life Technologies, Lot# 07F2235 K), 1 mM sodium puryvate (Life Technologies), 100 units/mL penicillin and 100 μg/mL streptomycin (Pen Strep, Gibco® Life Technologies) were added to DMEM. The pH was set at 7.4 ± 0.1, adjusted by adding appropriate amounts of 5 vol.% NaOH, when necessary.

Histidine (L-histidine monohydrochloride monohydrate, puriss p.a.) and copper nitrate ($Cu(NO_3)_2$, puriss p.a.) were obtained from Sigma–Aldrich, Sweden.

Phosphate buffered saline (PBS, pH 7.4) was prepared by mixing 8.77 g/L NaCl, 1.28 g/L Na_2HPO_4, 1.36 g/L KH_2PO_4, 370 μL/L 50% NaOH, pH 7.2–7.4 (all chemicals of analytical grade, Sigma–Aldrich, Sweden) in ultrapure water (18.2 MΩ cm, Millipore, Sweden).

All solution vessels were acid-cleaned in 10% HNO_3 for at least 24 h, and thereafter rinsed four times with ultrapure water.

2.2. Compositional analysis of the surface oxide

A Horiba Yvon Jobin HR800 Raman spectrometer was employed to study the surface oxide composition of the Cu NPs using a laser wavelength of 785 nm and a 50× objective. The laser beam was focused softly on a particle layer of Cu NPs to avoid beam damage. The layer was checked by optical microscopy before and after the measurements to assure no laser-induced damage. Three different areas (each with a diameter of approximately 10 μm) were investigated.

2.3. Particle size measurements

Particle size distribution measurements in solution were performed with a photon cross correlation spectroscopy instrument (Nanophox, Sympatec GmbH, Germany). The sample volume was 1 mL. All measurements were conducted at room temperature (20 ± 2 °C) in Eppendorf cuvettes (Eppendorf AG, Germany, UVette Routine pack, LOT no. C153896Q). A non-negative least square (NNLS) algorithm with a robust filter was used to obtain the intensity-weighed size distributions from the correlation functions. The sample solutions were prepared by adding 1 mg Cu NPs to 10 mL $DMEM^+$, where after the particle dispersion was sonicated for 3 min (Branson Sonifier 250, 30% duty cycle, output 4).

2.4. Zeta potential

The zeta potential (apparent surface charge) of the Cu NPs was studied using a Malvern Zetasizer nano Z instrument. The sample solutions were prepared by adding 1 mg Cu NPs to 10 mL NaCl (10 mM). The particle solution was there after sonicated for 3 min (Branson Sonifier 250, 30% duty cycle, output 4). The Smoluchowski approximation was used to calculate the zeta potential from the electrophoretic mobility of the particles in solution. A representative intensity distribution curve is given in Supporting information (Fig. S1).

2.5. Copper nanoparticles

Cu NPs, produced via wire explosion [30] were kindly provided by Ass. Prof. A. Yu. Godymchuk, Tomsk Polytechnic University, Russia. Detailed information on the particle characteristics is published elsewhere [16,28]. Briefly, the primary particle size is in the order of 50–200 nm and the surface oxide consists of a mixture of Cu_2O and CuO. These and additional characteristics are compiled in Fig. 1.

2.6. Copper nanoparticle exposures

5 mg Cu NPs were loaded into 50 mL solution and exposed at dark conditions at 37 °C for different time periods in a Stuart S180 incubator at bilinear shaking conditions (12°, 25 cycles/min). Triplicate samples and one blank sample without added Cu NPs were exposed. Directly after exposure, the samples were acidified to pH 2 using 65% HNO_3.

Ultracentrifugation (RCF 52900 *g*, Beckman Optima L-90K, SW-28 rotor) was employed for 1 h to separate the particle and the aqueous (released metals in solution) Cu-fractions. This procedure should remove all NPs sized approx. >20 nm from solution [31], which is larger than the primary size of the studied NPs [16]. A centrifugation time of 1 h exceeds the nominal exposure time, which means that some of the NPs were in solution and released Cu for a longer time period.

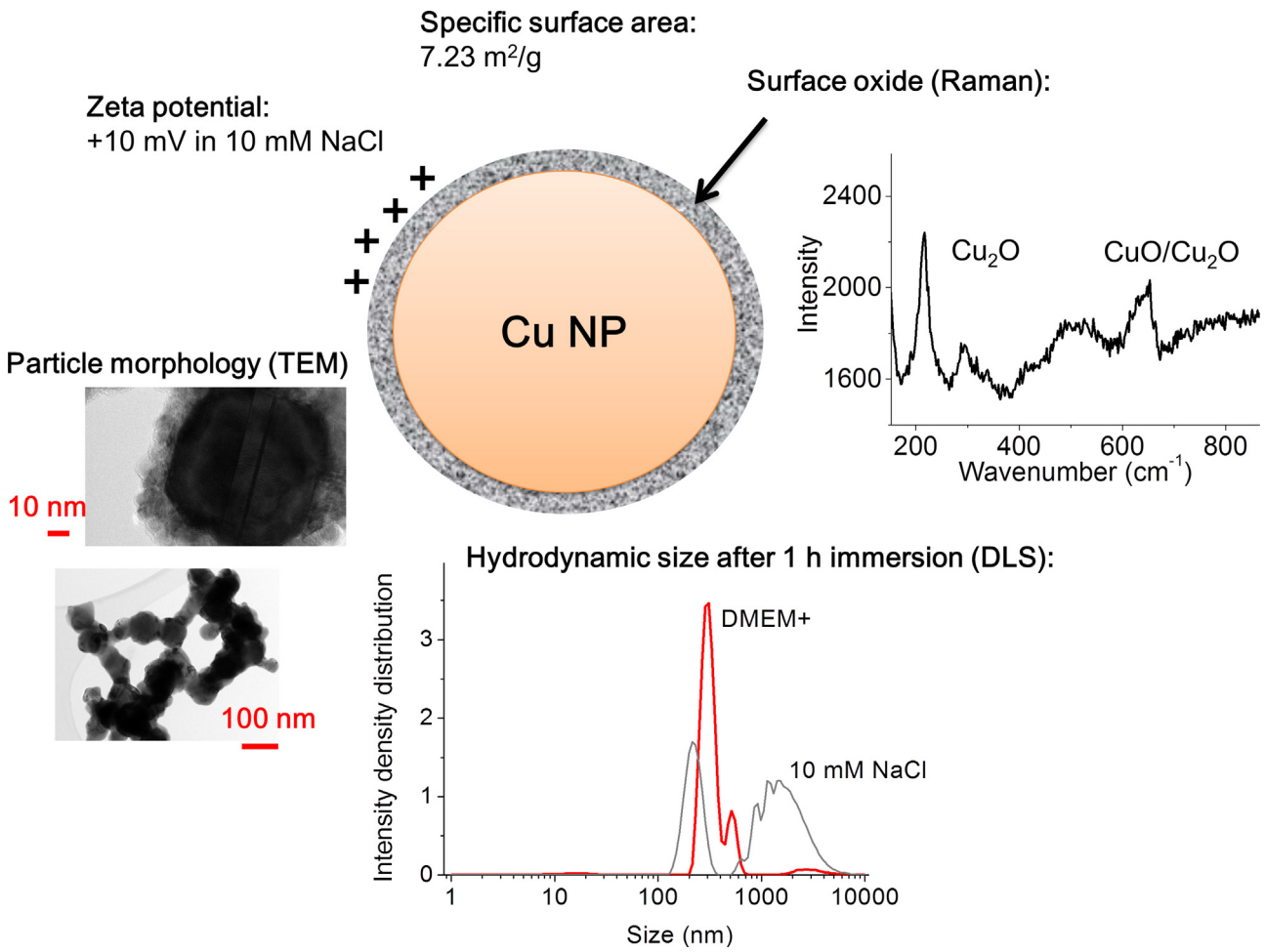

Fig. 1. Selected physico-chemical properties of the Cu NPs investigated in this study. Released Cu from Cu NPs is complexed to ligands in PBS, PBS + histidine, DMEM, and DMEM$^+$.

Investigations were performed to investigate if also Cu–protein bound species (present in FBS) could be removed by the centrifugation procedure as this would underestimate the amount of aqueous Cu. The same approach with similar loadings and exposure conditions as described above was therefore performed with Cu^{2+} ions (added as $Cu(NO_3)_2$) in DMEM$^+$. These tests showed no loss of Cu during the centrifugation process, thus no removal of Cu–protein bound species.

2.7. Copper concentration determination

Measurements of released Cu concentrations in solution were determined by means of atomic absorption spectroscopy (PerkinElmer AAnalyst 800 instrument in flame mode) using calibration standards at 0, 3, 10, 20, and 30 mg/L. Samples spiked with known amounts of Cu resulted in acceptable recoveries for all solutions and AAS methods (80–110%). The calibration curve was in all solutions linear to approximately 10 mg/L, with a deviation of approximately 10% at 30 mg/L (based on linear extrapolation from this 10 mg/L). The limit of detection (LOD) for the different solutions was estimated to 0.06 mg/L, the limit of identification (LOI) was 0.12 mg/L, and the limit of quantification (LOQ) was 0.18 mg/L, based on the method by Vogelgesang et al. [32].

Blank solutions (no Cu NPs) were measured for all experiments. Calibrations standards were measured regularly (every 6th sample) to detect possible calibration drifts. Recalibration was performed if a drift >5% was identified.

2.8. Contributing processes to released copper

The released amount of Cu in solution measured by means of AAS (Cu_{AAS}) originates from several different processes [33] (wear excluded at given conditions) as described in Eqs. (1) and (2):

$$Cu_{AAS} = Cu_{corrosion} + Cu_{oxide\ dissolution} + Cu_{background} - Cu_{precipitation} \quad (1)$$

$$Cu_{release} = Cu_{corrosion} + Cu_{oxide\ dissolution} \quad (2)$$

Corrosion-induced release of Cu ($Cu_{corrosion}$) is caused by Cu oxidation, usually a result of a defective or non-passive (ion-conductive) surface oxide. The chemical or electrochemical dissolution of the surface oxide ($Cu_{oxide\ dissolution}$) also result in the release of Cu. This process can be caused by protonation, reductive or oxidative dissolution of the surface oxide, or ligand-induced (complexation-induced) dissolution of the surface oxide, processes that all are adsorption-controlled and pH- and species-dependent [33]. The background concentration of Cu ($Cu_{background}$) is caused by contamination from chemicals, the equipment, or the air, and is usually in levels close to the detection limit as long as adequate cleaning procedures have been used. In this study, the background concentration was determined from parallel blank measurements. Released Cu that had precipitated ($Cu_{precipitation}$) and been centrifuged from the solution after exposure, or precipitated during exposure, was not measured by AAS.

Measured background concentrations in the blank solutions (if >0 mg/L) were subtracted from the measured concentrations from samples exposed to the Cu NPs. In this study, all sample

concentrations significantly exceeded the blank concentrations. Release data presented in this study is hence calculated according to Eq. (3) and presented as mean values of triplicate samples.

$$\frac{Cu_{AAS}\left(mg/L\right) - Cu_{background}\left(mg/L\right) \times Volume\,(L)}{added\ NP\ mass\ (mg)} \quad (3)$$

2.9. Electrochemical investigations

A carbon paste electrode (CPE) using graphite powder was employed for the electrochemical investigation using a Ag/AgCl (saturated KCl) reference electrode (Radiometer, Sweden) and a platinum wire as counter electrode. The working electrode (connected to the platinum wire) was made up of approximately 100 mg graphite powder mixed with 1.1 mg Cu NPs. The graphite powder was purchased from Alfa Aesar (99.9995% metal basis). The solution volume was approximately 3 mL and the pH was set to 7.4 ± 0.1. Additional details of the experimental setup are given elsewhere [34].

2.10. Statistical analysis

The double-sided Student's *t*-test was used (unequal variance, unpaired samples) to investigate significant differences in measured Cu concentrations between different samples. The *p*-value <0.05 was used as an estimate to determine whether the samples were significantly different from each other or not.

2.11. Speciation of released Cu species

The speciation of released Cu from the Cu NPs in the different media was determined using a Metrohm 797 VA Computrace polarographic instrument. An Ag/AgCl (3 M KCl) reference electrode and a platinum reference counter electrode were used together with a hanging mercury electrode as the working electrode. Solutions with released Cu from the Cu NPs were frozen directly after exposure, and thawed immediately before the polarography investigations. Prior to measurements, the solutions were degassed for 10 min with argon gas.

Differential pulse cathodic stripping voltammetry was then employed, with an accumulation time of 20 s at 0.1 V. Stripping was performed from 0.1 V to −1.2 V *vs.* Ag/AgCl, with a scan rate of 0.012 V/s, a voltage step time of 0.5 s, a voltage step of 0.0059 V, and a pulse time of 0.04 s. In this way, different Cu species can be identified at different stripping voltage positions. To quantify the amount of Cu species in solution, standard addition of Cu^{2+} ions (added as $Cu(NO_3)_2$) was performed three times to each sample. Two replicas were investigated for each addition. The detection limit was 0.5 μg/L and the determination limit 2 μg/L [32].

In addition, UV–vis spectroscopy was used to study the speciation of released Cu-species in solution using a JASCO V-630 (Easton, USA) instrument. A scan rate of 1000 nm/min, a bandwidth of 1.5 nm, and Plastibrand cuvettes (Wertheim, Germany) with cell lengths of 10 mm were used. A calibration curve was constructed using a Cu standard (1 g/L, PerkinElmer, Sweden) in the studied solutions to quantify the UV–vis results. The calibration curve was linear in the investigated concentration range (R^2 = 0.99). The detection limit was estimated to 1 mg/L, and the determination limit was 3 mg/L [32].

2.12. Chemical equilibrium modeling

The Joint Expert Speciation Software (JESS, version 8.3) was used for chemical equilibrium calculations [35,36]. The redox potential of the different solutions, measured with an Inlab redox electrode (Mettler Toledo, Sweden) and calibrated using standard solutions from Thermo Scientific, Sweden (Lot # 967961), varied between 260 and 360 mV (*vs.* Ag/AgCl). As the chemical speciation modeling results were not largely affected by differences in redox potential for this interval, a potential of 305 mV was selected for all predictions.

For predictions in PBS, input data on the free concentrations of the components of the respective medium were the same as in the release and cell experiments. In the case of DMEM, a few components (choline, pantothenate, niacinamide, inositol) were not available in the JESS database, and hence not included in the calculations. All other input data for the modeling are presented in Tables S4 (Supporting information) together with the free concentrations of the solution components.

2.13. Measurements of reactive oxygen species

The 2′,7′-dichlorofluorescein diacetate (DCFH-DA) assay was used to measure acellular ROS production. In brief, sodium hydroxide (0.01 M) was added to DCFH-DA to cleave the DA from the DCFH after which the reaction was stopped by the addition of PBS. This solution was then incubated with Cu NPs in particle concentrations of 50 and 100 μg/mL (prepared as described below) and 15 μM DCFH for 30 min. Fluorescence (excitation 485 nm, emission 535 nm) was then recorded using a plate reader (VICTOR^{3}V 1420 Multilabel counter, Perkin Elmer). To prepare solutions of the released Cu fraction, the diluted particle suspensions were incubated for 2 h at 37 °C (briefly mixed two times during the incubation) followed by centrifugation at a RCF of 16060 *g* for 15 min.

2.14. Cell membrane damage

A549 type II epithelial cell lines (obtained from the American Type Culture Collection) were grown in DMEM supplemented with 10% fetal bovine serum in a humidified atmosphere at 37 °C and 5% CO_2. The cells were seeded in 24-well plates the day before the experiment (see image in Fig. S2). Immediately before exposure, a stock suspension (1 mg/mL) of Cu NPs (or Cu ions—from $Cu(NO_3)_2$) was prepared in de-ionized water and sonicated for 15 min in a water bath. The stock suspension was then diluted to the final particle concentration in the various solutions (PBS, PBS + histidine, DMEM and DMEM$^+$). The cells were exposed to a final volume of 0.5 mL in the 24-well plates. Cell membrane damage was then assessed using Trypan blue staining. In this method, compromised cell membranes are stained blue whereas cells with intact cell membranes are not. The percentage of stained cells is analyzed microscopically. This robust procedure is described in detail elsewhere [28]. The choice of this method is based on findings from our previous study [16] in which different methods for analyzing membrane damage were investigated. This study concluded *e.g.,* that the commonly used LDH-assay was not appropriate to use due to particle-assay interactions.

3. Results and discussion

3.1. Particle characteristics

Selected characteristics of the Cu NPs are schematically compiled in Fig. 1. The surface oxide has a thickness in the order of 10–30 nm, consisting of Cu_2O and CuO. The primary particle size is in the range between 50 and 200 nm [16]. Dynamic light scattering (DLS) measurements revealed hydrodynamic particle sizes in the order of 300 nm after 1 h immersion in DMEM$^+$ (ionic strength of 130 mM), and evident particle agglomeration with time. When compared to a non-biomolecule containing medium of lower ionic strength (10 mM NaCl), particle agglomeration was even more pronounced. This reflects the stabilizing effect of adsorbed

biomolecules onto the Cu NPs in DMEM$^+$. More information, *e.g.*, detailed TEM images, is given elsewhere [16,28].

3.2. The release kinetics of Cu from Cu NPs are linked to both oxide dissolution and corrosion

Fig. 2a depicts the kinetics of aqueous Cu species released from Cu NPs in DMEM$^+$, DMEM, PBS + histidine, and PBS. Corresponding time-dependent changes in OCP (open circuit potential) of the Cu NPs are displayed in Fig. 2b for each case. The amount of released Cu in solution is higher in the media containing amino acids and/or proteins compared with PBS. These findings are in agreement with previous investigations [21,28]. The presence of histidine in solution has previously been shown to enhance the release of Cu from CuO NPs more than other amino acids [21]. This enhancement is likely related to its capability of forming stable complexes with Cu [37].

The OCP of the Cu NPs starts at a potential (*approx.* 0.1 V *vs.* Ag/AgCl sat. KCl) close to what is expected for CuO (see Supporting information, Fig. S3) and is reduced during the first hours of immersion in DMEM$^+$ and PBS + histidine to a level of approximately −0.07 to −0.1 V (*vs.* Ag/AgCl). This potential range coincides with the expected potential for Cu metal at pH 7.4 [38]. Cu as particles or the size of the Cu NPs (>100 nm) are not expected to significantly influence the OCP levels in comparison with bulk Cu [39]. The observed drop in OCP hence indicates that the surface oxide of the Cu NPs undergoes dissolution in DMEM$^+$ and PBS + histidine, resulting in particles that are less protected by the surface oxide (reduced passivity) and that corrode at a relatively constant rate after a few hours (2–7 h). A similar drop in OCP has also been observed for stainless steel upon addition of bovine serum albumin (BSA) [40]. This drop was correlated with an increased amount of released metals and explained by a de-stabilizing effect of the surface oxide induced by BSA [40]. The hypothesis of oxide dissolution during the first

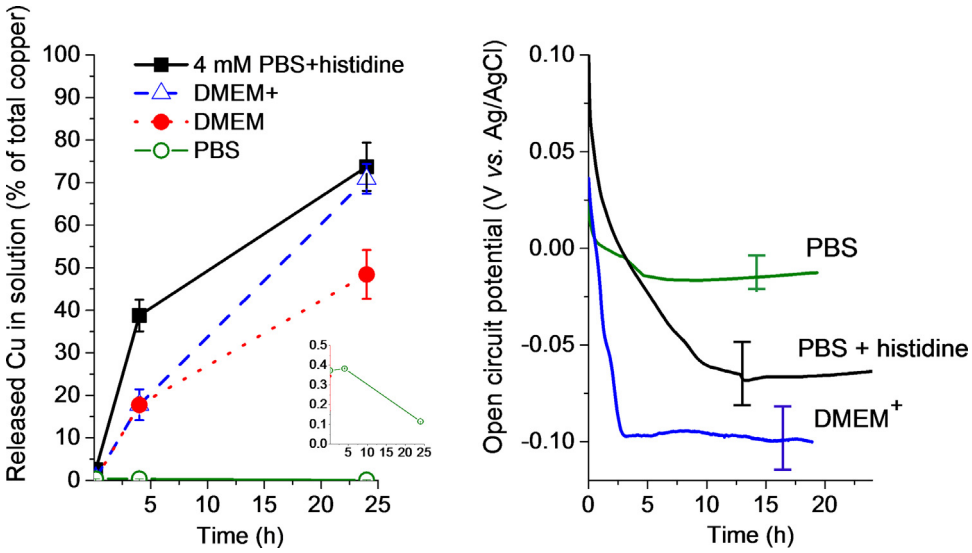

Fig. 2. (a) Kinetics of total aqueous Cu released from Cu NPs in PBS + histidine, DMEM, DMEM$^+$ and PBS, as measured by AAS. Error bars represent one standard deviation from three independent samples. The inset magnifies the low amount of aqueous Cu observed in PBS. (b) Time-dependent changes in OCP for Cu NPs in PBS, Histidine and DMEM$^+$ as deduced by CPE. Error bars represent one standard deviation from at least two independent samples.

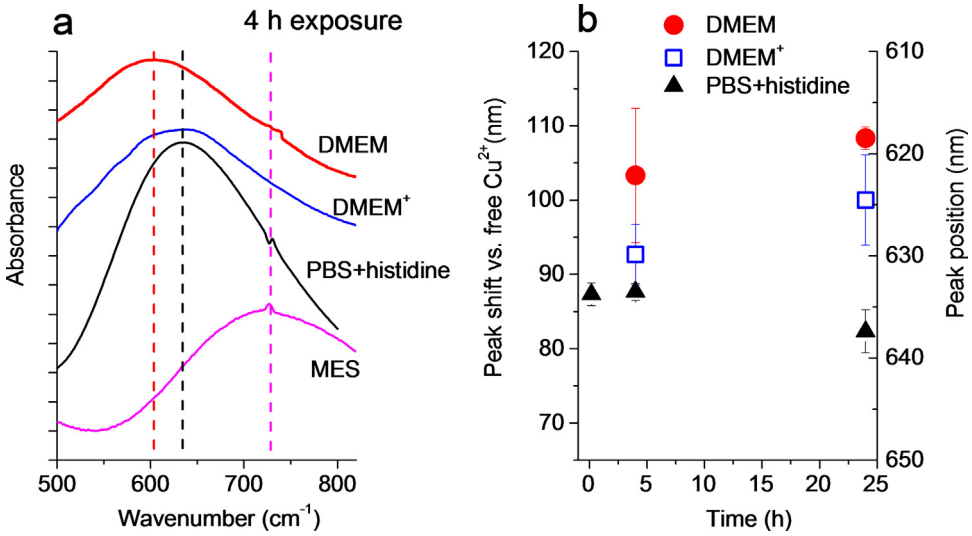

Fig. 3. (a) UV–vis spectra for released aqueous Cu species after 4 h exposure in 4 mM PBS + histidine, DMEM, and DMEM+, respectively. The exposed Cu NP loadings were 0.1 g/L, and the solutions were centrifuged to separate particles and aqueous species. The spectrum for free Cu^{2+}, added as $Cu(NO_3)_2$, in MES buffer (5 mM MES) is shown as a reference. The spectra have been offset for clarity and dotted lines have been added as a guide for the band positions. (b) Band positions in the different media shown as the shift *vs.* the free Cu^{2+} band, and also as absolute positions. Error bars represent one standard deviation, derived from three independent samples.

hours of exposure is further supported by findings of this study, as measured amounts of released Cu in solution from the Cu NPs during the first hours of exposure in PBS + histidine and DMEM$^+$ were in the same order of magnitude as would be the case given complete dissolution of the surface oxide (Fig. S4). It is expected that the biomolecules in PBS + histidine, DMEM, and DMEM$^+$ solutions interact and adsorb onto the Cu NPs [6,41–43]. Hence, enhanced amounts of released Cu in solution and the parallel drop in OCP in solutions containing biomolecules indicate that the adsorbed biomolecules (the protein corona) assist in activating the surface, *e.g.*, *via* ligand exchange reactions [21,43]. Since the OCP is influenced by (i) oxide dissolution, (ii) adsorbed species, and (iii) copper corrosion, we cannot determine whether the oxide is completely or almost completely dissolved after the first hours of exposure. This is followed by relatively constant corrosion rates, also indicated by the continuous copper release, (Fig. 2a).

A correlation between the OCP and the release of Cu was also evident in PBS, though less pronounced. This is seen as a small drop in OCP and very low amounts of released Cu. The largest changes in OCP and Cu release took place within the first minutes of exposure.

3.3. Released Cu from Cu NPs forms complexes with ligands present in PBS, PBS + histidine, DMEM, and DMEM$^+$

UV–vis spectra of the different solutions with different amounts of released Cu (Cu NPs separated) are displayed in Fig. 3. A spectrum of free Cu ions (Cu^{2+}) in MES buffer (2-(*N*-morpholino)ethanesulfonic acid), which is a non-Cu binding medium [44], is included for comparison. Shifts in band positions (blue-shifts) compared to the band position of free Cu^{2+} ions (MES buffer) in the biomolecule-containing solutions indicate complexation between Cu^{2+} and ligands in histidine + PBS, DMEM, and DMEM$^+$. The blue shift hence provides information on the type of Cu-complexation [45]. Observed bands are displayed in Fig. 3a after 4 h of exposure, in addition to observed band shifts in relation to the peak of free Cu^{2+} ions for up to 24 h of exposure, (Fig. 3b). Due to the low amounts of Cu released in PBS, no detectable band was observed in the UV–vis spectra for this solution.

From the band position at 637–642 nm, it is concluded that released Cu ions form complexes with histidine in the 4 mM PBS + histidine solution [37]. For DMEM, which contains 13 different amino acids, the band position is in the range between 610 and 630 nm. This position corresponds to complexes between Cu ions and a variety of possible amino acids, *e.g.*, lysine (620 nm) [45]. Cu–albumin complexes are in addition to Cu–amino acid complexes possible constituents in DMEM$^+$, since the band of the Cu–protein complexes, *e.g.*, Cu–albumin, overlaps with the band positions of amino acid of BSA in the 530–620 nm region [46]. No significant change with time in the release experiments was observed for the band positions of the differently formed Cu-complexes, (Fig. 3b). Moreover, no shifts in band positions were observed for equivalent additions of added free Cu^{2+} ions (as easily soluble $Cu(NO_3)_2$) compared with Cu released from the Cu NPs (data not shown).

Polarography (cathodic stripping voltammetry) was also employed to deduce the speciation of released Cu species. The peak positions of observed aqueous Cu species are presented in Fig. 4. Several peaks were observed in the voltammograms generated in DMEM and DMEM$^+$ (Fig. S5), indicative of different Cu-species in solution. Peaks in the −0.05 to −0.4 V range indicate complexation of Cu to amino acids, including Cu–histidine [37]. Both amino acids and proteins are expected to contribute with peaks in the −0.5 to −0.95 V range [47–49]. Peaks corresponding to Cu–cystine [50] and Cu–albumin [49] species have for instance been reported in this potential range. However, the overlap between possible Cu species of the many constituents in DMEM and DMEM$^+$ hinders any detailed assignment of the peaks. Similar to the UV–vis findings, no peaks were assigned to free Cu ions (Cu^{2+}) in the media containing biomolecules as compared with reference measurements in MES buffer. The observed peak position was in PBS though very close to observations in MES, which then tentatively was assigned as a labile Cu–phosphate complex. This observation implies that released Cu from Cu NPs forms labile complexes in PBS compared with more strongly bound complexes formed in the biomolecule-containing media.

Species identified in the UV–vis and polarography measurements were quantified. The total concentration of observed Cu species after 4 h of immersion was not significantly different ($p > 0.05$) for any of the time periods for the total amount of released amount of Cu in solution determined by means of AAS (Fig. 5). This supports the conclusion of complete complexation of released Cu into solution from the Cu NPs with ligands in the biomolecule-containing media. The same results were observed after 10 min and 24 h of immersion, see Fig. S6 (supporting information). The amount of Cu in PBS, quantified by means of polarography, was significantly lower than measured with AAS. This difference is likely due to the formation of non-electroactive Cu–phosphate complexes, which are not possible to observe by means of polarography. Their possible formation is discussed below.

Chemical equilibrium modeling (JESS) were performed to predict the relative distribution of different Cu species in the different

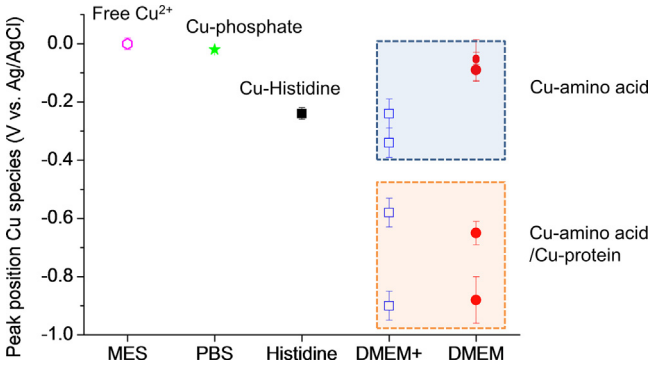

Fig. 4. Peak positions of Cu species released from Cu NPs (10 min, 4 h, and 24 h exposure in PBS, 4 mM PBS + histidine, DMEM, and DMEM$^+$. Peak positions in MES buffer (5 mM MES) with added $Cu(NO_3)_2$ (1 mg/L) are shown for comparison. Error bars represent one standard deviation from three independent samples.

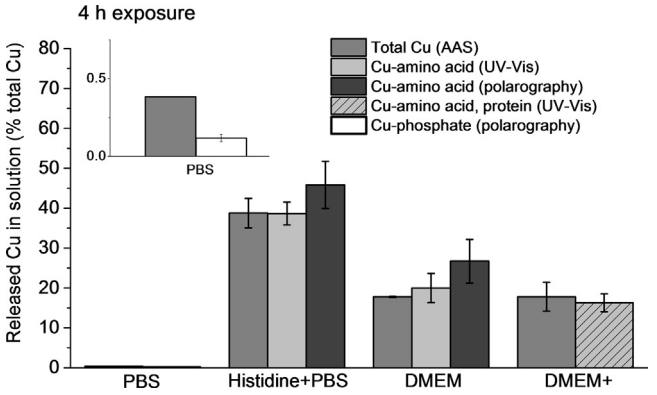

Fig. 5. Summary of quantification results from AAS, UV–vis, and cathodic stripping voltammetry of released Cu species from Cu NPs exposed for 4 h in PBS, PBS + histidine, DMEM and DMEM$^+$, respectively. The total amount of added Cu (as Cu NPs) was 0.1 g/L. Error bars represent one standard deviation of three independent samples. The inset shows a magnification of aqueous Cu species in PBS. DMEM$^+$ was excluded in the polarography quantification as the response was not linear to added Cu. This can be attributed to *e.g.*, the lack of electro activity of some of the Cu–albumin complexes formed [54].

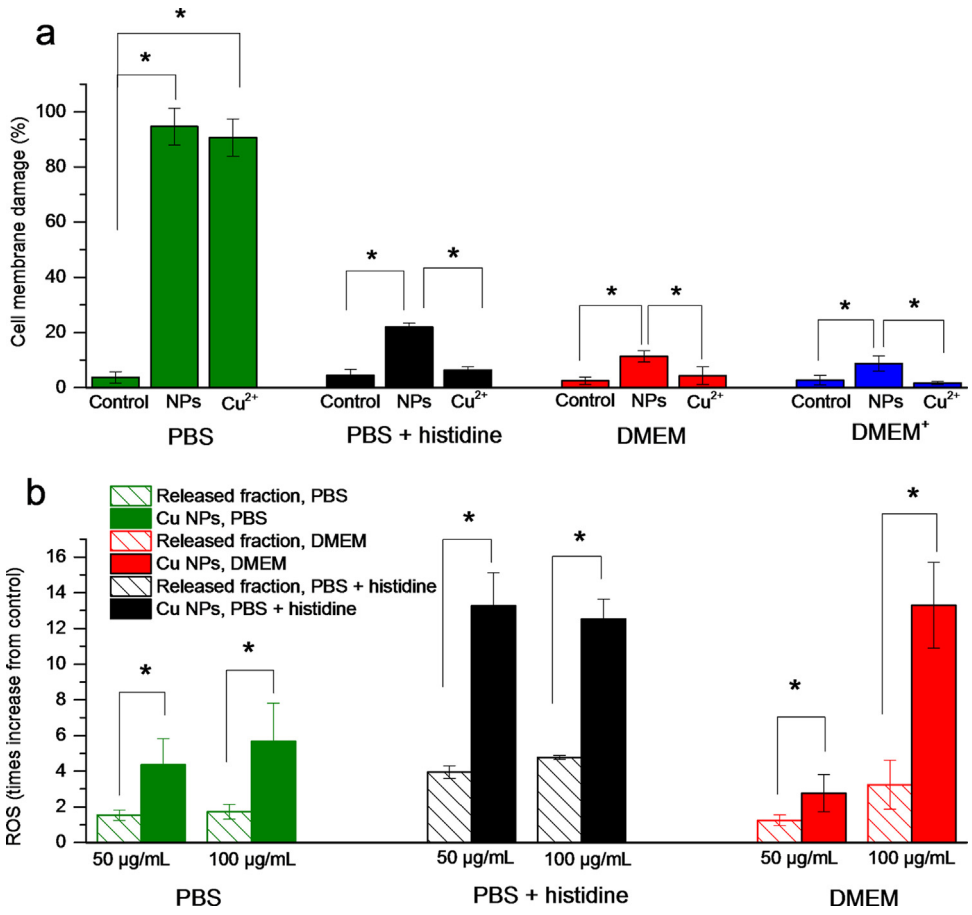

Fig. 6. (a) Membrane damage analyzed using Trypan blue staining as a result of A549 cell exposure to Cu NPs in PBS, PBS + histidine, DMEM and DMEM$^+$. The total added amount of Cu (as Cu NPs) was 25 μg/mL. The membrane damage was assessed after 2 h exposure. Asterisks (*) indicate significant differences ($p < 0.05$) for each solution. Error bars indicate the standard deviation from two independent experiments. (b) ROS production (after 30 min incubation in DCHF-DA) for the released Cu fraction only (without Cu NPs), and for Cu NPs (the released fraction + Cu NPs), all in the absence of cells. The Cu NPs were exposed for 2 h in their respective medium before introducing DCHF-DA. For the release fraction only, the NPs were removed by centrifugation before introducing DCFH-DA. The asterisk (*) indicates a significant difference ($p < 0.05$) between the released fraction and the Cu NPs.

media based on the total amount of released Cu in solution, as determined by means of AAS after 10 min, 4 h, and 24 h of exposure (see Tables S1–S3). The JESS modeling results show that the formation of a single Cu–histidine complex was prevalent in PBS + histidine, while an array of different Cu–amino acid complexes were possible constituents in DMEM. The JESS modeling results thus support the experimental findings of UV–vis and polarography, and are qualitatively in agreement with reported predictions of Cu speciation in blood plasma [35]. The modeling furthermore shows (Table S3) that labile Cu–phosphate complexes are expected to form in PBS. However, the amount of Cu in PBS is close to saturation (see Fig. S7). These results are in line with the results from AAS that show a reduced amount of Cu in solution over time, indicative of slow precipitation of formed complexes (Fig. 2a). Precipitation of complexes is further corroborated by findings with polarography, as the technique is only able to detect electro-active species (not solid Cu–phosphate). These analyses revealed lower concentrations of a Cu–phosphate complex in solution compared with the total Cu concentration, as measured by means of AAS (Fig. 5).

No speciation predictions were performed for the DMEM$^+$ medium as the JESS model is currently only able to consider low weight biomolecules, not proteins [35]. However, it is anticipated that the speciation distribution of Cu is similar to the predictions made in DMEM, with the addition of complexes between protein and Cu as *e.g.*, BSA is known to form complexes with Cu [51].

Predictions of the fraction of free Cu^{2+} ions compared with the total concentration of Cu released into DMEM are depicted in Fig. S8. The results are comparable with background concentrations of free Cu^{2+} ions in blood plasma, $<10^{-11}$ M [52].

In all, it has been shown that released Cu from Cu NPs into the biomolecule-containing media (DMEM, DMEM$^+$, PBS + histidine) does not exist as free Cu^{2+} ions but forms essentially completely strongly bonded complexes with different biomolecules: (i) Cu is bound to histidine in PBS + histidine, mostly as 2:1 histidine–Cu complexes; (ii) to amino acids in DMEM (partially to sulfur groups in amino acids, mostly bound as 2:1 amino acid:Cu-complexes); and (iii) to amino acids and proteins (most probably albumin) in DMEM$^+$. In PBS, the non-biomolecule containing fluid, some labile Cu-complexes form in addition to a non-soluble Cu–phosphate complex that readily precipitates with time. This means that the total released amount of Cu in PBS is higher than what is measured in solution, *c.f.*, Eq. (1).

3.4. The formation of Cu–biomolecule complexes in solution strongly reduces the cell membrane damage induced by the released fraction of Cu species compared with free Cu ions

The cell membrane integrity of A549 cells in PBS, PBS + histidine, DMEM, and DMEM$^+$ (Fig. 6a), were investigated using the Trypan blue assay to deduce the role of solution composition, speciation of released Cu in solution and Cu NPs (25 μg/mL). Equivalent

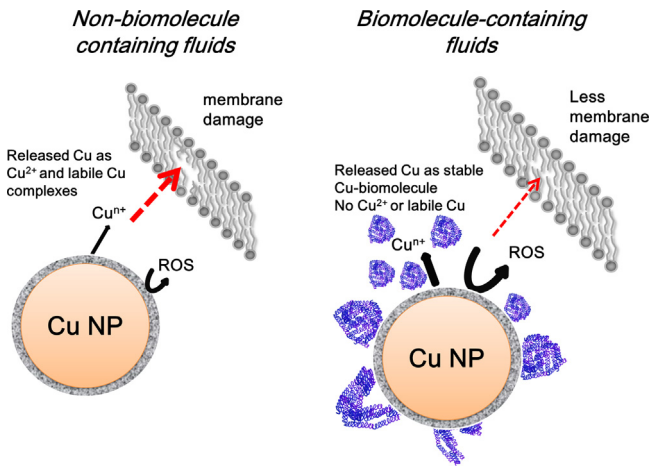

Fig. 7. A proposed model of Cu NP-induced membrane damage in media with ($DMEM^+$, DMEM, PBS + histidine) and without biomolecules (PBS).

molar amounts of added Cu^{2+} ions (from easily soluble $Cu(NO_3)_2$) were included for comparison. Additional data for a higher particle concentration (50 μg/mL) is provided in Fig. S9 (Supporting information). The results clearly show that massive cell membrane damage (>90%) was induced when cells were exposed in PBS, both for Cu NPs (which include Cu NPs and released labile Cu-complexes) and for added free Cu^{2+} ions. In the biomolecule-media, the membrane damage was reduced both for added Cu^{2+} ions and for the Cu NPs, compared with observations in PBS (Fig. 6a).

The extent of ROS production was investigated using the DCFH-DA method, for Cu NPs and the released Cu fraction, and for the released Cu fraction only (*i.e.,* Cu NPs diluted in the solution specified, incubated for 2 h in 37 °C and then centrifuged to remove the NPs). This was achieved via exposures at cell-free conditions in PBS, PBS + histidine, DMEM, and $DMEM^+$, Fig. 6b. ROS generation by the Cu NPs (including contribution from the released fraction as well as from the Cu NPs) was observed in all investigated fluids (Fig. 6b). However, in contrast to the membrane damage, the addition of the biomolecules led to higher levels of ROS formation. When comparing the Cu NPs and the released fraction it is obvious that the NPs were much more prone to generate ROS compared to the released Cu fraction. Measurements of the generation of ROS over time were also performed for other particle concentrations, showing the same trend (see Figs. S10 and S11).

Some of the authors have previously concluded that the released fractions of Cu species from NPs of both Cu and CuO have a minor, or non-significant, effect compared with the NPs on the observed toxicity [16,28]. Similar observations with small effects induced by the released Cu fraction have been reported by others [25,26,53]. Results of this study clearly show that the Cu species of the released fraction did not induce any membrane damage in the biomolecule-containing media due to the formation of Cu–biomolecule complexes and very low concentrations of free Cu^{2+} ions, whereas a small effect was observed in the presence of the Cu NPs. For added Cu^{2+} ions (from easily soluble $Cu(NO_3)_2$) to the biomolecule-containing media, rapid complexation of the Cu^{2+} ions explains the low membrane integrity damage observed. As a consequence of complexation of Cu^{2+} ions, the ROS production was reduced (Fig. 6b) [21,54].

A model of Cu NP-induced membrane damage is proposed in Fig. 7 based on all generated results. Corrosion reactions taking place at the surface of Cu NPs have previously been suggested to be linked to the extent of induced membrane damage in cell media [16,17]. We can now corroborate this hypothesis by showing that corrosion most likely takes place for the Cu NPs, seen in a drop in OCP and enhanced release of Cu in the biomolecule-containing media (Fig. 5). It is possible that the surface oxide of the Cu NPs also contributes to the generation of ROS. However, the authors have previously reported a higher production of ROS from Cu NPs (the same batch of particles as in this study) compared with NPs of CuO [55]. This can be linked to the observation of a higher extent of membrane damage and release of Cu into solution for Cu NPs compared with CuO NPs [16]. It is furthermore suggested that the surface oxide of the Cu NPs predominantly dissolves during the first few hours of immersion in biomolecule-containing media, from which follows a negligible effect of the surface oxide beyond this point in time (*c.f.*, OCP results) after which the corrosion rate is relatively constant. Corrosion reactions result in the production of ROS as intermediate reaction products (Fig. 6b) [17,56,57] that are known to induce cellular damage [14,58]. The interaction and adsorption of solution ligands from the biological media onto the oxidized surface of the Cu NPs are likely. However, their presence does not seem to inhibit the formation of ROS to any significant degree. Adsorbed layers, or patches, of the adsorbed biomolecules on the surface of the Cu NPs are hence not very dense and protective as findings reported by Shi et al. [57]. That study showed a reduced ROS production, and lower ability of surface oxidation of Cu NPs when using capping molecules to stabilize the particles in solution. The study compared long alkane chains with molecules of short carbon chain lengths (from mercaptocarboxylic acids).

Cellular uptake, rather than membrane interaction, has been suggested to play a more important role for CuO NPs compared with Cu NPs, which is likely related to the generally lower solubility of CuO NPs [23,55,59]. Therefore, future studies should include release and speciation investigations in order to take into account *e.g.,* internalized Cu, and therefore also consider other pH conditions and biological media (*e.g.,* simulating lysosomal fluids) than investigated in this study.

When the lung cells were exposed to Cu NPs in PBS, high membrane damage was induced by the Cu NPs in spite of their relatively minor corrosion and measured release of Cu. The labile complexes formed by released Cu in PBS are known to induce membrane damage directly [58,60,61]. This is corroborated by findings of this study with a high degree of induced membrane damage in PBS upon exposure to easily soluble Cu salt (Fig. 6a). It can also be noted that since the ROS levels were increased by the presence of Cu NPs in PBS (Fig. 6b), ROS could also contribute to the membrane damage. Precipitation of Cu-complexes can also play a role for the induced toxicity in PBS, as at least a non-soluble Cu–phosphate compound is likely to form (Figs. 5 and S7) that possibly may interact with the cells.

4. Conclusions

Speciation studies of Cu released from Cu NPs in biomolecule-containing media, *e.g.*, the commonly used cell medium DMEM, showed essentially no free Cu^{2+} ions in solution ($<10^{-11}$ M), as released Cu was completely complexed to biomolecules. This observation is valid up to a high investigated particle loading of 100 μg/mL, effectively showing that the released fraction, including effects of free Cu^{2+} ions, will not take any part for the membrane damage induced by the Cu NPs (*e.g.*, for the cell line A549 investigated in this study up to 24 h of exposure). The complexation of released Cu also inhibited ROS production. The membrane damage in the biomolecule-containing media (PBS + histidine, DMEM, and $DMEM^+$) was instead linked to corrosion reactions taking place at the surface of the Cu NPs that resulted in ROS formation. Corrosion was accelerated by the destabilizing effect of the biomolecules on the surface oxide, which dissolved during the first

hours in the biomolecule-containing media followed by relative constant corrosion rates.

The absence of biomolecules in PBS resulted in minor corrosion and ROS formation compared with corresponding effects in media containing biomolecules. Instead, released Cu from Cu NPs in PBS (via corrosion or oxide dissolution processes) formed labile Cu-complexes that were able to induce cellular damage directly. The role of Cu–phosphate precipitates cannot be excluded.

The different mechanisms of induced membrane damage of Cu NPs in PBS and biomolecule-containing media highlight the important influence of the buffer and medium used in tests of Cu NP toxicity.

In all, the benefit of using corrosion and speciation investigations for understanding acutely induced membrane damage by Cu NPs is highlighted. It is suggested that an array of techniques is used in nanotoxicological studies, *e.g.*, when screening NPs, to assess the correlation between particle properties and induced toxicity.

Acknowledgements

Maria-Elisa Karlsson and Sulena Pradhan, KTH, are gratefully acknowledged for performing CPE and DLS measurements, respectively. Frederik Mathiason, KTH, is gratefully acknowledged for performing the Cu release studies. Francesca Cappelini, KI, is acknowledged for help with the ROS studies. The Swedish National Research Council (VR, grant number 2013-5621), and Göran Gustafsson's foundation are acknowledged for financial support. The work forms part of the Mistra Environmental Nanosafety program financed by the Swedish Foundation for Strategic Environmental Research. Prof. Peter May, University of Murdoch, Australia, is highly acknowledged for giving insights on how to operate the JESS modeling software.

Appendix A. Supplementary data

Supplementary data associated with this article can be found, in the online version, at http://dx.doi.org/10.1016/j.colsurfb.2016.01.052.

References

[1] V.H. Grassian, When size really matters: size-dependent properties and surface chemistry of metal and metal oxide nanoparticles in gas and liquid phase environments, J. Phys. Chem. C 112 (2008) 18303–18313.
[2] G. Oberdörster, E. Oberdörster, J. Oberdörster, Nanotoxicology: an emerging discipline evolving from studies of ultrafine particles, Environ. Health Perspect. 113 (2005) 823–839.
[3] G.V. Lowry, K.B. Gregory, S.C. Apte, J.R. Lead, Transformations of nanomaterials in the environment, Environ. Sci. Technol. 46 (2012) 6893–6899.
[4] H.L. Karlsson, Å. Holgersson, L. Möller, Mechanisms related to the genotoxicity of particles in the subway and from other sources, Chem. Res. Toxicol. 21 (2008) 726–731.
[5] W.M. Lee, Y.J. An, H. Yoon, H.S. Kweon, Toxicity and bioavailability of copper nanoparticles to the terrestrial plants mung bean (*Phaseolus radiatus*) and wheat (*Triticum aestivum*): plant agar test for water insoluble nanoparticles, Environ. Toxicol. Chem. 27 (2008) 1915–1921.
[6] Q. Mu, G. Jiang, L. Chen, H. Zhou, D. Fourches, A. Tropsha, B. Yan, Chemical basis of interactions between engineered nanoparticles and biological systems, Chem. Rev. 114 (2014) 7740–7781.
[7] A. Nel, T. Xia, L. Mädler, N. Li, Toxic potential of materials at the nanolevel, Science 311 (2006) 622–627.
[8] G. Oberdörster, Safety assessment for nanotechnology and nanomedicine: concepts of nanotoxicology, J. Intern. Med. 267 (2010) 89–105.
[9] D.H. Nies, Microbial heavy-metal resistance, Appl. Microbiol. Biotechnol. 51 (1999) 730–750.
[10] D.M. Di Toro, H.E. Allen, H.L. Bergman, J.S. Meyer, P.R. Paquin, R.C. Santore, Biotic ligand model of the acute toxicity of metals. 1. Technical basis, Environ. Toxicol. Chem. 20 (2001) 2383–2396.
[11] H. Hasman, M.J. Bjerrum, L.E. Christiansen, H.C.B. Hansen, F.M. Aarestrup, The effect of pH and storage on copper speciation and bacterial growth in complex growth media, J. Microbiol. Methods 78 (2009) 20–24.
[12] S. Lin, A.A. Taylor, Z. Ji, C.H. Chang, N.M. Kinsinger, W. Ueng, S.L. Walker, A.E. Nel, Understanding the transformation, speciation, and hazard potential of copper particles in a model septic tank system using zebrafish to monitor the effluent, ACS Nano 9 (2015) 2038–2048.
[13] T. Theophanides, J. Anastassopoulou, Copper and carcinogenesis, Crit. Rev. Oncol. Hematol. 42 (2002) 57–64.
[14] F. Li, C. Lei, Q. Shen, L. Li, M. Wang, M. Guo, Y. Huang, Z. Nie, S. Yao, Analysis of copper nanoparticles toxicity based on a stress-responsive bacterial biosensor array, Nanoscale 5 (2013) 653–662.
[15] N. von Moos, V.I. Slaveykova, Oxidative stress induced by inorganic nanoparticles in bacteria and aquatic microalgae-state of the art and knowledge gaps, Nanotoxicology 8 (2014) 605–630.
[16] H.L. Karlsson, P. Cronholm, Y. Hedberg, M. Tornberg, L. De Battice, S. Svedhem, I. Odnevall Wallinder, Cell membrane damage and protein interaction induced by copper containing nanoparticles—importance of the metal release process, Toxicology 313 (2013) 59–69.
[17] B.A. VanWinkle, K.L. de Mesy Bentley, J.M. Malecki, K.K. Gunter, I.M. Evans, A. Elder, J.N. Finkelstein, G. Oberdörster, T.E. Gunter, Nanoparticle (NP) uptake by type I alveolar epithelial cells and their oxidant stress response, Nanotoxicology 3 (2009) 307–318.
[18] G. Applerot, J. Lellouche, A. Lipovsky, Y. Nitzan, R. Lubart, A. Gedanken, E. Banin, Understanding the antibacterial mechanism of CuO nanoparticles: revealing the route of induced oxidative stress, Small 8 (2012) 3326–3337.
[19] R. Drouin, H. Rodriguez, S.-W. Gao, Z. Gebreyes, T.R. O'Connor, G.P. Holmquist, S.A. Akman, Cupric ion/ascorbate/hydrogen peroxide-induced DNA damage: DNA-bound copper ion primarily induces base modifications, Free Radical Biol. Med. 21 (1996) 261–273.
[20] S. Stohs, D. Bagchi, Oxidative mechanisms in the toxicity of metal ions, Free Radical Biol. Med. 18 (1995) 321–336.
[21] Z. Wang, A. Von Dem Bussche, P.K. Kabadi, A.B. Kane, R.H. Hurt, Biological and environmental transformations of copper-based nanomaterials, ACS Nano 7 (2013) 8715–8727.
[22] M. Kalbacova, S. Roessler, U. Hempel, R. Tsaryk, K. Peters, D. Scharnweber, J.C. Kirkpatrick, P. Dieter, The effect of electrochemically simulated titanium cathodic corrosion products on ROS production and metabolic activity of osteoblasts and monocytes/macrophages, Biomaterials 28 (2007) 3263–3272.
[23] P. Cronholm, H.L. Karlsson, J. Hedberg, T.A. Lowe, L. Winnberg, K. Elihn, I. Odnevall Wallinder, L. Möller, Intracellular uptake and toxicity of Ag and CuO nanoparticles: a comparison between nanoparticles and their corresponding metal ions, Small 9 (2013) 970–982.
[24] A.M. Studer, L.K. Limbach, L. Van Duc, F. Krumeich, E.K. Athanassiou, L.C. Gerber, H. Moch, W.J. Stark, Nanoparticle cytotoxicity depends on intracellular solubility: comparison of stabilized copper metal and degradable copper oxide nanoparticles, Toxicol. Lett. 197 (2010) 169–174.
[25] J. Gonzalez-Estrella, D. Puyol, S. Gallagher, R. Sierra-Alvarez, J.A. Field, Elemental copper nanoparticle toxicity to different trophic groups involved in anaerobic and anoxic wastewater treatment processes, Sci. Total Environ. 512 (2015) 308–315.
[26] C. Gunawan, W.Y. Teoh, C.P. Marquis, R. Amal, Cytotoxic origin of copper(II) oxide nanoparticles: comparative studies with micron-sized particles, leachate, and metal salts, ACS Nano 5 (2011) 7214–7225.
[27] R.J. Griffitt, R. Weil, K.A. Hyndman, N.D. Denslow, K. Powers, D. Taylor, D.S. Barber, Exposure to copper nanoparticles causes gill injury and acute lethality in zebrafish (*Danio rerio*), Environ. Sci. Technol. 41 (2007) 8178–8186.
[28] K. Midander, P. Cronholm, H.L. Karlsson, K. Elihn, L. Möller, C. Leygraf, I. Odnevall Wallinder, Surface characteristics, copper release, and toxicity of nano- and micrometer-sized copper and copper(II) oxide particles: a cross-disciplinary study, Small 5 (2009) 389–399.
[29] Y. Hedberg, M. Norell, P. Linhardt, H. Bergqvist, I. Odnevall Wallinder, Influence of surface oxide characteristics and speciation on corrosion, electrochemical properties and metal release of atomized 316L stainless steel powders, Int. J. Electrochem. Sci. 7 (2012) 11655–11677.
[30] A. Russkikh, R. Baksht, A.Y. Labetskiĭ, P. Levashov, S. Tkachenko, K. Khishchenko, A. Shishlov, A. Fedyunin, S. Chaĭkovskiĭ, Effect of the high-voltage electrode polarity and wire preheating on the energy characteristics of electric explosion of fine tungsten wires in vacuum, Plasma Phys. Rep. 32 (2006) 823–835.
[31] T.M. Tsao, Y.M. Chen, M.K. Wang, Origin, separation and identification of environmental nanoparticles: a review, J. Environ. Monit. 13 (2011) 1156–1163.
[32] J. Vogelgesang, J. Hädrich, Limits of detection, identification and determination: a statistical approach for practitioners, Accredit. Qual. Assur. 3 (1998) 242–255.
[33] Y.S. Hedberg, I. Odnevall Wallinder, Metal release from stainless steel in biological environments: a review, Biointerphases 11 (2016) 018901–018917.
[34] P. Linhardt, Corrosion of metals in natural waters influenced by manganese oxidizing microorganisms, Biodegradation 8 (1997) 201–210.
[35] P.M. May, JESS at thirty: strengths, weaknesses and future needs in the modelling of chemical speciation, Appl. Geochem. 55 (2015) 3–16.
[36] P.M. May, K. Murray, JESS, a joint expert speciation system—I. Raison d'être, Talanta 38 (1991) 1409–1417.
[37] P. Deschamps, P. Kulkarni, M. Gautam-Basak, B. Sarkar, The saga of copper(II)–L-histidine, Coord. Chem. Rev. 249 (2005) 895–909.
[38] M. Pourbaix, Atlas of Electrochemical Equilibria. 1974 in Aqueous Solutions, NACE, Houston, Texas, 1974, pp. 1974.
[39] W. Plieth, Electrochemical properties of small clusters of metal atoms and their role in the surface enhanced Raman scattering, J. Phys. Chem. 86 (1982) 3166–3170.

[40] Y. Hedberg, X. Wang, J. Hedberg, M. Lundin, E. Blomberg, I. Odnevall Wallinder, Surface-protein interactions on different stainless steel grades: effects of protein adsorption, surface changes and metal release, J. Mater. Sci.: Mater. Med. (2013) 1–19.
[41] C.C. Fleischer, C.K. Payne, Nanoparticle–cell interactions: molecular structure of the protein corona and cellular outcomes, Acc. Chem. Res. 47 (2014) 2651–2659.
[42] E.M. Marti, C. Methivier, P. Dubot, C. Pradier, Adsorption of (S)-histidine on Cu(110) and oxygen-covered Cu(110), a combined Fourier transform reflection absorption infrared spectroscopy and force field calculation study, J. Phys. Chem. B 107 (2003) 10785–10792.
[43] L.-F. Wang, N. Habibul, D.-Q. He, W.-W. Li, X. Zhang, H. Jiang, H.-Q. Yu, Copper release from copper nanoparticles in the presence of natural organic matter, Water Res. 68 (2015) 12–23.
[44] H.E. Mash, Y.-P. Chin, L. Sigg, R. Hari, H. Xue, Complexation of copper by zwitterionic aminosulfonic (good) buffers, Anal. Chem. 75 (2003) 671–677.
[45] E. Prenesti, P. Daniele, M. Prencipe, G. Ostacoli, Spectrum–structure correlation for visible absorption spectra of copper(II) complexes in aqueous solution, Polyhedron 18 (1999) 3233–3241.
[46] Y. Zhang, D.E. Wilcox, Thermodynamic and spectroscopic study of Cu(II) and Ni(II) binding to bovine serum albumin, J. Biol. Inorg. Chem. 7 (2002) 327–337.
[47] P. Deschamps, N. Zerrouk, T. Martens, M.-F. Charlot, J. Girerd, J. Chaumeil, A. Tomas, Copper complexation by amino acid: L-glutamine–copper (II)–L-histidine ternary system, J. Trace Microprobe Tech. 21 (2003) 729–741.
[48] J.C. Moreira, A.G. Fogg, Determination of nanomolar levels of histidine by differential-pulse adsorptive-cathodic stripping voltammetry of its copper(II) complex, Analyst 115 (1990) 41–43.
[49] M. Studničková, J. Pitřincová, J. Kovář, The electrochemical behaviour of copper proteins using differential pulse polarography, Bioelectrochem. Bioenerg. 25 (1991) 109–120.
[50] M.T. Stankovich, A.J. Bard, The electrochemistry of proteins and related substances: I. Cystine and cysteine at the mercury electrode, J. Electroanal. Chem. Interfacial Electrochem. 75 (1977) 487–505.
[51] P.Z. Neumann, A. Sass-Kortsak, The state of copper in human serum: evidence for an amino acid-bound fraction, J. Clin. Invest. 46 (1967) 646–658.
[52] P.M. May, P.W. Linder, D.R. Williams, Computer simulation of metal-ion equilibria in biofluids: models for the low-molecular-weight complex distribution of calcium(II), magnesium(II), manganese(II), iron(III), copper(II), zinc(II), and lead(II) ions in human blood plasma, J. Chem. Soc., Dalton Trans. 6 (1977) 588–595.
[53] H.J. Jo, J.W. Choi, S.H. Lee, S.W. Hong, Acute toxicity of Ag and CuO nanoparticle suspensions against *Daphnia magna*: the importance of their dissolved fraction varying with preparation methods, J. Hazard. Mater. 227 (2012) 301–308.
[54] A.M. Wade, H.N. Tucker, Antioxidant characteristics of L-histidine, J. Nutr. Biochem. 9 (1998) 308–315.
[55] Y. Rodhe, S. Skoglund, I. Odnevall Wallinder, Z. Potácová, L. Möller, Copper-based nanoparticles induce high toxicity in leukemic HL60 cells, Toxicol. In Vitro 29 (2015) 1711–1719.
[56] M. Genshaw, A. Damjanovic, J.M. Bockris, Hydrogen peroxide formation in oxygen reduction at gold electrodes: I. Acid solution, J. Electroanal. Chem. Interfacial Electrochem. 15 (1967) 163–172.
[57] M. Shi, H.S. Kwon, Z. Peng, A. Elder, H. Yang, Effects of surface chemistry on the generation of reactive oxygen species by copper nanoparticles, ACS Nano 6 (2012) 2157–2164.
[58] K. Jomova, S. Baros, M. Valko, Redox active metal-induced oxidative stress in biological systems, Transition Met. Chem. 37 (2012) 127–134.
[59] P. Cronholm, K. Midander, H.L. Karlsson, K. Elihn, I. Odnevall Wallinder, L. Möller, Effect of sonication and serum proteins on copper release from copper nanoparticles and the toxicity towards lung epithelial cells, Nanotoxicology 5 (2011) 269–281.
[60] M. Suwalsky, B. Ungerer, L. Quevedo, F. Aguilar, C. Sotomayor, Cu^{2+} ions interact with cell membranes, J. Inorg. Biochem. 70 (1998) 233–238.
[61] J. Hall, Cellular mechanisms for heavy metal detoxification and tolerance, J. Exp. Bot. 53 (2002) 1–11.